

Charge separation effects in solid targets and ion acceleration with a two-temperature electron distribution

M. Passoni,^{1,2,3} V. T. Tikhonchuk,² M. Lontano,³ and V. Yu. Bychenkov⁴

¹*Dipartimento di Ingegneria Nucleare, Politecnico di Milano, Milan, Italy*

²*Centre Lasers Intenses et Applications, UMR 5107 CNRS–Université Bordeaux I–CEA, Université Bordeaux I, 33405 Talence Cedex, France*

³*Istituto di Fisica del Plasma, CNR, Milan, Italy*

⁴*P. N. Lebedev Institute, Russian Academy of Sciences, 53 Leninskii Prospect, Moscow 119991, Russia*

(Received 5 August 2003; published 27 February 2004)

The electrostatic field at the solid-vacuum interface generated by two electron populations with different thermal energies, each following a Boltzmann distribution, is analytically derived from the Poisson equation and studied in terms of plasma parameters. In particular, the effect of the pressure of each of the two populations on the amplitude of the electric field and on its spatial extension is described. In order to evaluate the cold electron temperature, an analytical model for the Ohmic heating of the background electron population by laser generated fast electrons is developed and the consequences on ion detachment, ionization, and acceleration processes in laser-solid experiments are discussed. The efficiency of ion acceleration is shown to be controlled by the heating rate of the background electrons.

DOI: 10.1103/PhysRevE.69.026411

PACS number(s): 52.38.Kd, 52.50.Nr

I. INTRODUCTION

Recent experiments have demonstrated the possibility to accelerate ions to high energies through the interaction of an intense and short laser pulse with a thin solid target. These ion beams have attractive and peculiar characteristics, such as high collimation, high particle flux, and a short time duration. Several possible applications of these laser-produced ion beams have been suggested: they have already been used as a diagnostic tool in laser-plasma interaction experiments [1]; they also reveal themselves useful in the implementation of the fast ignition concept, with high energy beams of light ions generated in laser-solid interaction [2–4], in material science [5], as injectors for ion accelerators [6,7] and for the production of short-lived isotopes for medical diagnostics [8,9], and in the hadron therapy [10,11].

Laser-solid interaction experiments at the 100 TW power level produce up to 10^{13} protons with the energy spectrum ranging from a few MeV to a few tens MeV [12–14]. Metallic as well as insulator targets were used, with a thickness range from a few μm up to more than 100 μm . Two types of laser pulses have been used in these experiments: either single-shot pulses of a picosecond duration and energy of the order of 100 J or much shorter pulses of the order of a few tens of femtoseconds with energy of about 1 J. The second type of pulses is more interesting for applications since such lasers are less expensive, more compact, and can operate with the repetition rate of the order of 1 Hz or more. It is important for the various applications mentioned above to understand the role of target and laser parameters in the process of ion acceleration in order to control the characteristics of ion beams.

The origin of the observed accelerated ions and the mechanism of acceleration are still the matters of debate. Ions are created and accelerated either at the front surface, directly illuminated by the laser, as argued in Refs. [12] and

[15–17], or at the rear surface, through the self-consistent electrostatic accelerating field. There is no definitive answer to the question of the spatial origin of the ions, since experimental observations by different groups do not converge yet to a unique and coherent picture [15,18]. It is likely that the particular experimental conditions (above all, the prepulse and target surface properties) play a fundamental role. However, in some experiments [13,19] it has been demonstrated unambiguously that physical processes on the rear surface are particularly important.

Theoretically, the problem of ion acceleration on the rear surface in laser-solid experiments has been first described in terms of quasineutral plasma expansion in vacuum [20,21]. In these descriptions the plasma is assumed to have a single-temperature electron population in thermodynamical equilibrium. However, in the subpicosecond regime, the inertia of ions is important and the assumption of quasineutrality must be abandoned in order to give a better description of the process. Nonquasineutral plasma expansion has been considered in Refs. [22–28] within the hypothesis of a single-temperature electron population. Two-temperature electron distributions have been considered in Refs. [29–33] with the assumption of the plasma quasineutrality.

The experiments on ultraintense and ultrashort laser pulse interaction with solid targets evidence that the electron population produced at the rear target surface can be characterized at least by two temperatures, one describing the presence of hot electrons accelerated by the laser field, while the other refers to the much colder electron distribution of the target electrons. The hot electron component is created directly by the laser pulse in the plasma plume at the front surface of the target. It forms a beam propagating normally to the target surface with the divergence between 3° and 15° . The density of this electron population is of the order of the critical density (10^{20} – 10^{21} cm^{-3}) and its temperature is of the order of the laser ponderomotive potential (\sim MeV for the relativistic-

tically intense pulses). It contains up to 20%-30% of the laser energy.

The free motion of this hot electron beam through the target requires the presence of a return current which locally compensates the flow of the hot (and fast) electron component. The return current in metallic targets is provided by the conduction electrons which are put in motion by the electric field generated by the fast electrons. In insulators, the background free electron population is created by field and thermal ionization. Since the density of the background electron population in both cases is of the order of the solid density, that is, much bigger than the fast electron density, the required velocity for current neutralization is small and their temperature is much lower than that of the hot electrons. However, this cold and dense electron population can be ohmically heated by the return current [34].

In this paper, we investigate the features of the electrostatic field created by a two-temperature electron population at the rear side of a solid target. As compared with previous analytical treatments, our aim is to study in more detail the electric field on the rear surface of a solid thin film created by a propagating relativistic electron beam. We also develop an analytical model of heating of the cold electron population by the return current and analyze the consequences of these processes on the ion acceleration.

The paper is organized as follows. In Sec. II the electrostatic field at the rear surface of the target is found and the role of the two electron populations is analyzed. In Sec. III our model is completed by an analytical description of the Ohmic heating of the background electron population in a metal. The effects of a two-Maxwellian electron distribution and Ohmic heating of the cold population on ion acceleration are discussed in Sec. IV. Section V is devoted to concluding remarks and summary.

II. THE CHARGE SEPARATION EFFECTS

Generation of high energy electrons by the laser pulse interacting with a thin solid foil breaks plasma quasineutrality and generates a strong electric field at the rear side of the target.

In this section we present an analytical one-dimensional model describing the electrostatic field at the solid-vacuum interface generated by two-electron populations with different thermal energies, each following the Boltzmann distribution. Certain aspects of this model are also discussed in Ref. [35], where it is considered as the initial plasma state for Vlasov-Poisson numerical simulations of the plasma expansion.

A. Electric field equations

Here we consider a plasma constituted by the cold ions and two-electron populations with different thermal energies and look for the self-consistent electrostatic field $E = -\partial_x \phi$ generated in this system. The ions are supposed to be cold and at rest with a step-function density distribution, that is, $n_i = n_{0i}$ for $x \leq 0$ and $n_i = 0$ for $x > 0$, where the x axis is directed normally to the target surface. We assume that the densities of both electron populations, hot and cold, n_{eh} and

n_{ec} , depend on the spatial coordinate x , while their temperatures, T_h and T_c , are constants. The electrons follow Boltzmann distributions $n_{eh(c)} = n_{0h(c)} \exp(e\phi/T_{h(c)})$, where $n_{0h(c)}$ is the unperturbed hot (cold) electron densities. The electrostatic potential ϕ satisfies the Poisson equation

$$\partial_x^2 \phi = 4\pi e(n_{eh} + n_{ec} - Zn_i), \quad (1)$$

where Z is the effective ion charge state in the solid. The quasineutrality of the unperturbed plasma, $n_{0h} + n_{0c} = Zn_{0i}$, sets the boundary conditions for the electric field and the potential in the solid at $x \rightarrow -\infty$: $\partial_x \phi(-\infty) = \phi(-\infty) = 0$. At the vacuum side, there are no particles and no electric field, that is, $\partial_x \phi(\infty) = 0$. We note, incidentally, that the choice of Boltzmann electron distributions implies $\phi(\infty) \rightarrow -\infty$ and results in a divergent final kinetic energy for a particle in such a field. This is a source of problems in the quantitative estimate of the final energy of accelerated ions. This issue is discussed in more detail elsewhere [27,36].

According to Eq. (1), inside the target, for $x < 0$, the electrostatic potential is described by the following Poisson-Boltzmann equation:

$$\partial_x^2 \phi = 4\pi e(n_{0h} e^{e\phi/T_h} + n_{0c} e^{e\phi/T_c} - Zn_{0i}). \quad (2)$$

By defining the parameters $a \equiv n_{0c}/n_{0h}$ and $b \equiv T_c/T_h$, one can write the first integral of Eq. (2):

$$\lambda_{dh}^2 (\partial_x \phi)^2 = 2[\exp\phi + ab \exp(\phi/b) - (1+ab) - (1+a)\phi], \quad (3)$$

where $\varphi \equiv e\phi/T_h$ is the dimensionless potential and $\lambda_{dh} = (T_h/4\pi n_{0h} e^2)^{1/2}$ is the unperturbed hot electron Debye length. The solution of Eq. (3) is then found in implicit form

$$\int_{\varphi(0)}^{\varphi(x)} \frac{d\varphi}{[\exp\varphi + ab \exp(\varphi/b) - (1+ab) - (1+a)\varphi]^{1/2}} = -\sqrt{2} \frac{x}{\lambda_{dh}}, \quad (4)$$

where $\varphi(0)$ is the (dimensionless) electrostatic potential in $x=0$, to be determined. Moreover, far from the plasma surface the arguments φ and φ/b are ‘‘sufficiently small,’’ and one can expand the exponentials in Eq. (4) up to second-order terms; therefore, the explicit solution of the problem is found:

$$\varphi \approx \varphi(0) \exp\left[\left(1 + \frac{a}{b}\right)^{1/2} \frac{x}{\lambda_{dh}}\right]. \quad (5)$$

Outside the plasma, for $x > 0$, the Poisson-Boltzmann equation for the dimensionless potential φ reads

$$\lambda_{dh}^2 \partial_x^2 \varphi = \exp\varphi + a \exp(\varphi/b), \quad (6)$$

which admits the first integral

$$\lambda_{dh}^2 (\partial_x \varphi)^2 = 2[\exp\varphi + ab \exp(\varphi/b)] \quad (7)$$

and the consequent implicit solution

$$\int_{\varphi(0)}^{\varphi(x)} \frac{d\varphi}{[\exp\varphi + ab\exp(\varphi/b)]^{1/2}} = -\sqrt{2} \frac{x}{\lambda_{dh}}. \quad (8)$$

Taking the limits $a \rightarrow 0$ and $b \rightarrow 1$ in Eqs. (4) and (8), which correspond physically to consider a single-temperature electron population, we recover the results given in Refs. [23] and [28].

The electrostatic potential $\varphi(0)$ and the electric field $E(0)$ at $x=0$, where the latter reaches a maximum, can be determined by requiring the continuity of the potential and of the electric field, in $x=0$. Solving the system for $\varphi(0)$ and $\partial_x \varphi(0)$, obtained by evaluating Eqs. (3) and (7) at $x=0$, one gets for the potential at the solid-vacuum interface

$$\varphi(0) = -\frac{1+ab}{1+a} \quad (9)$$

and using the definitions of a and b , the dimensional form of this result reads

$$e\phi(0) = -\frac{T_h n_{0h} + T_c n_{0c}}{n_{0h} + n_{0c}} = -\frac{\sum_{\alpha=h,c} p_{0\alpha}}{\sum_{\alpha=h,c} n_{0\alpha}} = -\langle T_{0e} \rangle, \quad (10)$$

where the unperturbed hot and cold electron pressures, p_{0h} and p_{0c} , have been introduced and the mean electron temperature $\langle T_{0e} \rangle$ is weighted on the unperturbed densities.

The maximum electric field $E(0)$ is now given by

$$E(0) = \sqrt{2} \frac{T_h}{e\lambda_{dh}} \left\{ \exp\left[-b\left(\frac{1+ab}{b+ab}\right)\right] + ab \exp\left(\frac{1+ab}{b+ab}\right) \right\}^{1/2}. \quad (11)$$

This equation is written in terms of the physical quantities b and ab , which are the ratio between the two electron temperatures and the ratio between the two unperturbed electron pressures, respectively.

Below we aim to analyze the main features of the self-consistent electrostatic field. In particular, we are interested in the dependences of the maximum value and spatial profiles of this electric field on the ‘‘cold’’ and ‘‘hot’’ electron physical parameters (temperatures and pressures).

B. Dependence of the maximum electric field on the electron parameters

The maximum value of the resulting electric field is given by Eq. (11). We assume that the hot electron temperature is much greater than the cold electron temperature and vice versa for the electron density, that is, $b \ll 1$ and $a \gg 1$, which correspond to laser pulse interaction with solid targets. Let us study the following three physical regimes: hot pressure much greater than cold pressure ($ab \ll 1$); cold pressure much greater than hot pressure ($ab \gg 1$); hot and cold pressures of the same order ($ab \approx 1$).

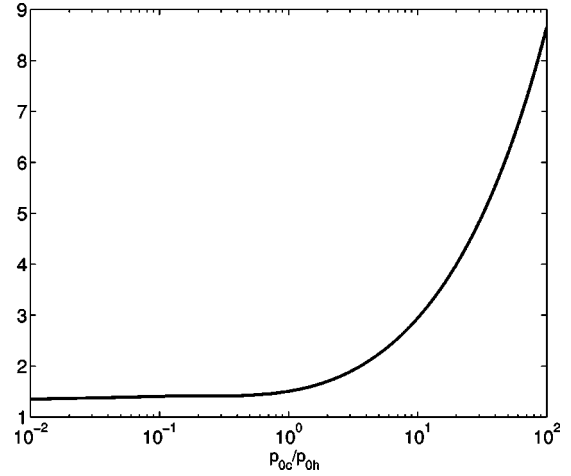


FIG. 1. Maximum value of the electric field $\bar{E}(0)$, normalized to $T_h/e\lambda_{dh}$, as a function of the cold-to-hot electron pressure ratio $ab = p_{0c}/p_{0h}$; for $ab \lesssim 1$, $\bar{E}(0) \approx \sqrt{2}$, while the behavior for $ab > 1$ is approximately given by $\bar{E}(0) \approx \sqrt{(2/e)ab}$.

If the hot pressure is greater than the cold pressure, that is, $ab \ll 1$, the maximum electric field is approximately given by

$$E(0) \cong \sqrt{2} \frac{T_h}{e\lambda_{dh}} \left[\exp\frac{1}{2} \left(\frac{b}{b+ab} \right) \right] \rightarrow \sqrt{2} \frac{T_h}{e\lambda_{dh}}. \quad (12)$$

In the opposite limit, $a \ll 1$, the maximum electric field would be $E(0) \rightarrow \sqrt{2/e}(T_h/e\lambda_{dh})$, recovering again the one-temperature result [23,28] (note the difference, in the last and following expressions, between the Nepero’s number e and the electric charge e).

In the opposite case, when the cold pressure is greater than the hot pressure, $ab \gg 1$, we can approximate $E(0)$ as

$$E(0) \cong \sqrt{\frac{2}{e} ab} \frac{T_h}{e\lambda_{dh}} = \sqrt{\frac{2}{e} \frac{T_c}{e\lambda_{dc}}}, \quad (13)$$

where we have introduced the unperturbed cold electron Debye length $\lambda_{dc} = (T_c/4\pi n_{0c}e^2)^{1/2}$. We see from these expressions that in this regime the maximum field is dominated by the parameters of the cold population: in particular, it depends only on the cold electron pressure (while, for a given value of the cold electron pressure p_{0c} , it does not depend appreciably on the cold electron temperature T_c).

Finally, if the cold and hot electron pressures are of the same order, $ab \approx 1$, the maximum electric field is roughly given by

$$E(0) \sim \sqrt{2} \frac{T_h}{e\lambda_{dh}}. \quad (14)$$

In Fig. 1 the maximum value of the electric field $E(0)$, normalized to $T_h/e\lambda_{dh}$, is shown as a function of the electron pressure ratio ab .

The performed study demonstrates that it is possible to increase the maximum electric field by the cold electron pressure boost for a given hot electron pressure, because

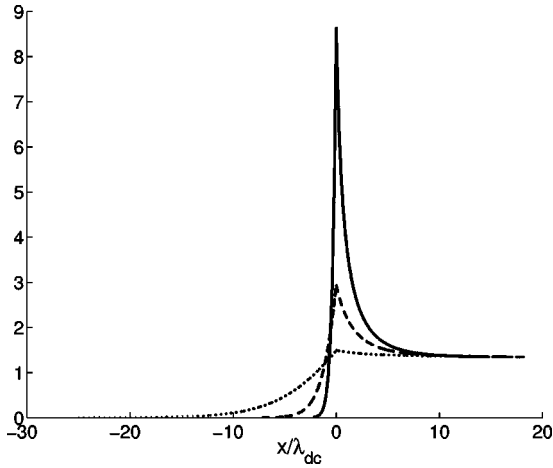


FIG. 2. Electric field profiles $\bar{E}(x)$, normalized to $T_h/e\lambda_{dc}$, for cold-to-hot electron temperature ratio $b=T_c/T_h=0.01$ and for cold-to-hot electron pressure ratio $ab=p_{0c}/p_{0h}=1$ (dotted line), $ab=10$ (dashed line), and $ab=100$ (solid line). The x coordinate is normalized to the cold electron Debye length λ_{dc} corresponding to $ab=10$.

roughly $E(0) \approx \sqrt{8\pi(n_{0c}T_c + n_{0h}T_h)}$. This could be achieved by energy exchange between the two electron populations, where a small decrease in the hot electron temperature may significantly increase the cold one, and the cold electron pressure as well. This scenario is explored in the following section.

C. Dependence of the electric field spatial profile on the electron parameters

Let us now consider the spatial characteristics of the self-consistent electrostatic field. $E(x)$ is given by Eqs. (4) and (8), inside the target and in vacuum, respectively. Again we consider the limits $b \ll 1$ and $a \gg 1$, and study how the field profile varies by changing the pressure of the two electron populations.

In Figs. 2 and 3, the electric field is shown as a function of the spatial coordinate x . The cold electron population determines the spatial penetration of the electric field inside the solid target: by rising the cold pressure for a given hot electron pressure and a given temperature ratio (and consequently reducing λ_{dc}), although the peak field increases as shown in Fig. 1, the field drops more and more sharply, almost exponentially, inside the target from the maximum value to zero over a few cold electron Debye lengths, as it is clearly evident in Fig. 2. Equation (5) justifies explicitly this fact. Indeed, the field inside the target, derived by the approximated explicit solution given in Eq. (5), has the following behavior:

$$E(x) \sim \exp\left(\frac{x}{\lambda_{dc}}\right), \quad (15)$$

even if we must observe that the approximation coming from the expansion of the exponential is not always good, very close to the plasma surface.

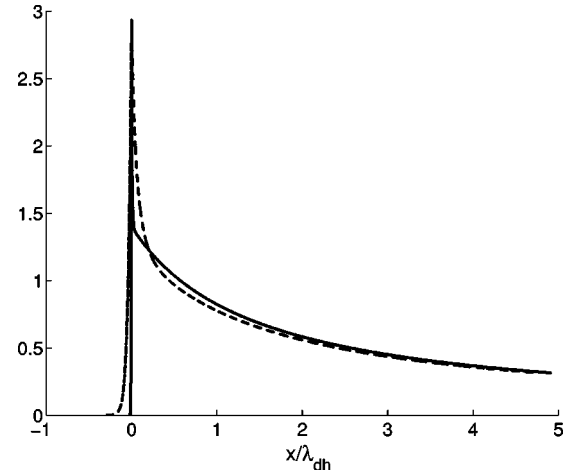


FIG. 3. Electric field profiles $\bar{E}(x)$, normalized to $T_h/e\lambda_{dh}$, for cold-to-hot electron pressure ratio $ab=p_{0c}/p_{0h}=10$ and for cold-to-hot electron temperature ratio $b=T_c/T_h=0.01$ (solid line) and $b=0.1$ (dashed line). The x coordinate is normalized to the hot electron Debye length λ_{dh} .

The cold electron population might have a sufficient energy to invade appreciably also the region outside the target. Thus it influences the spatial structure of the electric field over a distance of a few cold Debye lengths. We have seen in Sec. II B that under these conditions there is an increase in the maximum value achieved by the electric field, that is, the field peaks up around the solid-vacuum interface, as it is evident in Figs. 2 and 3. Outside the target, at a distance exceeding few cold Debye lengths, the electric field structure is then dominated by the hot population. In this last region, one can derive an approximate analytical solution for $E(x)$ starting from Eq. (8), neglecting the terms due to the cold population. Omitting the term $ab\exp(\varphi/b)$ in the square root of Eq. (8), after integrating one has

$$\varphi \cong -2 \ln \left[\exp[-\varphi(0)/2] + \frac{x}{\sqrt{2}\lambda_{dh}} \right].$$

Correspondingly, the electric field is

$$E(x) \cong \sqrt{2} \frac{T_h}{e\lambda_{dh}} \frac{1}{\exp[-\varphi(0)/2] + x/\sqrt{2}\lambda_{dh}}. \quad (16)$$

In particular, around the solid-vacuum interface, considering only the contribution from the hot electrons (that is, in the region after few cold electron Debye lengths, $x \gg \lambda_{dc}$), Eq. (16) gives

$$E \approx \sqrt{2} \frac{T_h}{e\lambda_{dh}} \exp\left(-\frac{b}{2} \frac{1+ab}{b+ab}\right) \rightarrow \sqrt{2} \frac{T_h}{e\lambda_{dh}}, \quad (17)$$

where the last limiting value holds always, provided that $b \ll 1$ and $a \gg 1$. Figures 2 and 3 illustrate the features of the self-consistent electric field for the case where the cold electron pressure is greater than the hot electron pressure. In particular, the correctness of Eqs. (13)–(17) is clearly seen.

It follows from this analysis that it is important to know the temperature and the pressure of the cold electron population because these quantities significantly influence both the maximum value of the electric field on the rear surface of the solid thin target and its spatial extension. To this aim, a model for the cold electron population heating in metal targets is presented in the following section.

III. THE MODEL OF BACKGROUND ELECTRON HEATING

The efficiency of the energy transfer from the laser-triggered hot electrons to the electric field and, consequently, the efficiency of successive ion acceleration depends on the efficiency of the cold electron heating due to the current neutralization in the target [34]. This is because of the cold electron pressure boost that, according to the results of Sec. II, increases the amplitude of the electric field. In order to estimate the pressure of the cold electron population we consider the heating of the background electrons in a metal target by the return current appeared as the plasma response to the laser-triggered fast electron flux. We describe an analytical model for the heating process in Secs. III A and III B, while a numerical example for aluminum target is presented in Sec. III C.

A. Basic equations

When a beam of fast electrons enters a target, it creates electric and magnetic fields which strongly affect electron transport. Hot electrons can propagate through metals because conduction electrons are put in motion by the fields, which cause a return current to appear, providing both charge and current neutralization. Background electrons are then ohmically heated due to the finite electrical resistivity of the target.

To evaluate the heating of the background electron population, we start following an approach proposed by Davies [37]. We will describe the response of the cold target electrons to the fast electron beam current by means of the basic Ohm's law

$$\mathbf{E} = \eta \mathbf{j}_c, \quad (18)$$

where \mathbf{E} and \mathbf{j}_c are the electric field and the current density inside the target, respectively, and η its electrical resistivity, which for simplicity is regarded as a scalar quantity. In this way, we are not describing the transient process of current neutralization, initially provided by the displacement current, and we are also neglecting plasma oscillations damped by collisions in the time scale of the plasma period of cold electrons. It has already been noted [37] that the time scales for these processes are extremely short, typically less than 1 fs. One can also simplify the full Maxwell equations. The magnetic diffusion time is a characteristic time scale for the return current decay. In metals, this is a relatively slow process, of the order of many tens of picoseconds [37]. Assuming the complete current neutralization, i.e., $\mathbf{j}_c \approx -\mathbf{j}$,

(being \mathbf{j} the fast electron current density), one finds $\mathbf{E} \approx -\eta \mathbf{j}$, and the Ohmic heating rate is ηj^2 .

The temporal evolution of the background electron temperature is described by the Fourier equation with the Ohmic heating source [37]. The heat conduction time scale depends on the background electron thermal conductivity κ_e and heat capacity per unit volume $C_e(T_e)$. Then the heat conduction time is given by

$$t_{heat} \approx L^2 C_e / \kappa_e, \quad (19)$$

where L is a characteristic length of the system—the transverse scale-length of the fast electron beam. One can assume this length to be of the same order of the laser pulse focal spot, that is, about $10 \mu\text{m}$. At room temperature, $T_e = T_{rm}$, t_{heat} is then of the order of tens of picoseconds, for typical values of thermal conductivity and heat capacity in metals (for example, for aluminum $t_{heat} \sim 10$ ps). Moreover, the coefficient of thermal conductivity κ_e depends on T_e . As we will see in greater detail below, in metals the femtosecond regime is characterized by strong electron-lattice nonequilibrium and in these conditions κ_e decreases with electron temperature as T_e^{-2} [38], resulting in a heat conduction time t_{heat} of the order of microseconds, for electron temperatures of the order of the Fermi temperature T_F in metals. Consequently, thermal conduction effects are expected to be even less important when the electron temperature T_e increase due to the Ohmic heating is accounted for. This conclusion is also in agreement with recent numerical simulations [39,40].

Generally speaking, the electrical resistivity η depends on both ion and electron temperatures. However, there is no direct heating of ions by the return current and the ion heating due to electron-ion energy exchange is negligible because its characteristic time is longer than 10 ps, which is out of the scope of our study. So we consider the ion temperature to be the room temperature during the heating process. With these assumptions the equation for the background electron temperature reads

$$C_e(T_e) \partial_t T_e = \eta(T_e) j^2. \quad (20)$$

In order to derive analytical scalings for the electron heating by the return current, we will assume a general power-law dependence of both the electrical resistivity

$$\eta = \eta_k (T_e / T_k)^\alpha \quad (21)$$

and the heat capacity

$$C_e(T_e) = C_k (T_e / T_k)^\beta \quad (22)$$

on the electron temperature T_e . Here, η_k and C_k are the electrical resistivity and the electron heat capacity at $T_e = T_k$, respectively. We choose T_k as the temperature at the initial time $t = t_k$. From Eqs. (20)–(22) we obtain an ordinary differential equation for the electron temperature, which can be analytically solved for a given time dependence of the hot electron current density. Because our model is not intended to be comprehensive, but rather to be restricted to a discussion of some new effects, we consider the simplest case $j = \text{const}$. With this position, for $\alpha - \beta < 1$, one finds the following solution:

$$T_e(t) = T_k \left[1 + \frac{\eta_{kj}^2}{\gamma C_k T_k} (t - t_k) \right]^\gamma, \quad (23)$$

where $\gamma = 1/(1 - \alpha + \beta)$. For $\alpha - \beta = 1$, instead of the algebraic dependence of Eq. (23), one has the exponential law for the electron heating:

$$T_e = T_k \exp \left[\frac{\eta_{kj}^2}{C_k T_k} (t - t_k) \right]. \quad (24)$$

Note that in the limit $\beta \rightarrow 0$ we recover the solutions found by Davies [37], who did not consider a possible temperature dependence of the electron heat capacity [41].

B. The heating of cold electrons by the return current

Let us now look in some details at the temperature dependence of heat capacity and electrical resistivity, starting from the former, $C_e(T_e)$. At temperatures well below the Fermi temperature, the conducting electrons are described as a free degenerate gas, with a resultant heat capacity varying linearly with the electron temperature. In particular, for a degenerate free electron gas we have [41]

$$C_{deg}(T_e) = \frac{\pi^2}{2} \frac{T_e}{T_F} n_e. \quad (25)$$

Above T_F , electrons behave approximately as a classical ideal gas, and the heat capacity in this case is no longer dependent on the electron temperature,

$$C_{id} = \frac{3}{2} n_e. \quad (26)$$

We characterize this behavior by splitting the electron temperature range into two different domains, setting in Eq. (22) $\beta = 1$ for $T_e < T_F$ and choosing the ideal value $\beta = 0$ for $T_e \geq T_F$. Note that in this way the corresponding heat capacity at room temperature t_{rm} is about three times less than the correct value given by Eq. (25). The temperature scaling of the heat capacity is summarized in Fig. 4.

We turn now to the electrical resistivity η . It is proportional to the electron collision frequency (i.e., inversely proportional to the electron relaxation time). The cold solid-state resistivity is mainly due to the electron-phonon scattering process, resulting in a linear dependence of the electrical resistivity on the ion temperature T_i (provided that $T_i \geq T_D$, where T_D is the Debye temperature of the conductor [41]). The electron-phonon collision frequency ν_{e-ph} is estimated as [41]

$$\nu_{e-ph} \cong g_0 \frac{T_i}{\hbar}, \quad (27)$$

where g_0 is a numerical factor of the order of unity. Another contribution to the total electron relaxation time comes from electron-electron collisions. The Fermi liquid theory of electrons in metals [41] predicts that the electron-electron collision frequency ν_{e-e} depends quadratically on the electron temperature T_e , and it can be estimated as

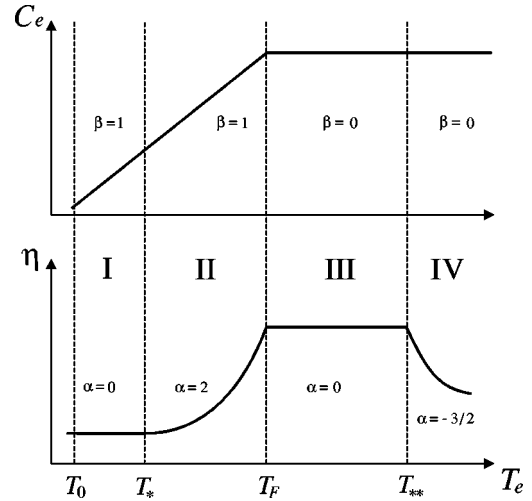


FIG. 4. Qualitative dependence of the cold electron heat capacity C_e and of the electrical resistivity η on the electron temperature, according to our model. The four domains of variations of the cold electron temperature, considered in the text, are shown.

$$\nu_{e-e} \cong \frac{T_e^2}{\hbar T_F}. \quad (28)$$

In the case of equilibrium between the electrons and the lattice, i.e., when $T_i = T_e$, electron-phonon collisions are the dominant process and electron-electron collisions can be neglected. However, the laser-solid interaction on femtosecond time scales is a strongly nonequilibrium process [38,42]. The ions remain much colder than the electrons, due to the relatively long electron-ion relaxation time, of the order of tens of picoseconds [42]. For this reason, at the subpicosecond time scale, the electron-phonon scattering process gives a temperature independent contribution to the electrical resistivity. This is why at the initial stage of the heating process the electrical resistivity is η_{rm} , the resistivity at room temperature T_{rm} . The electron-electron collisions are more and more frequent with increasing T_e . From Eqs. (27) and (28), one finds that the two collision frequencies ν_{e-ph} and ν_{e-e} become equal at the temperature [38]

$$T_* \cong (g_0 T_i T_F)^{1/2}. \quad (29)$$

Above the temperature T_* , the electron-electron collisions dominate, i.e., they contribute mainly to the electron relaxation time and, consequently, to the electrical resistivity. η increases up to a maximum value η_{max} and then saturates. This occurs when the electron mean free path becomes of the order of an interatomic distance [42,43]. Correspondingly, η_{max} can be deduced from Eq. (28) with $T_e \cong T_F$. Using the free electron gas model [41] and Eq. (28), one obtains

$$\eta_{max} = \frac{m_e}{n_e e^2} \frac{T_F}{\hbar}. \quad (30)$$

Indeed, it corresponds to the electrical resistivity where the relaxation time is taken to be equal to the plasma period of the background electrons. At higher temperatures, the elec-

trons behave like an ideal hot plasma, and the electron collision frequency is governed by the Spitzer law [44]:

$$\nu_{Spitzer} = \frac{4}{3} (2\pi)^{1/2} \frac{Ze^4 m_e n_e}{(m_e T_e)^{3/2}} \ln\Lambda, \quad (31)$$

where Z is the ionization degree and $\ln\Lambda$ is the Coulomb logarithm. From Eq. (31), the electrical resistivity decays as $T_e^{-3/2}$. The collision frequency given by Eq. (31) is of the order of the plasma frequency at the temperature T_{**} , which is of the order of $10T_F$. In the interval $T_F < T_e < T_{**}$, the plasma electrons are in the strongly coupled non-degenerate state. Following Ref. [42], in this interval we consider the electrical resistivity to be a constant. The temperature scaling of the electrical resistivity is summarized in Fig. 4.

According to the present model, four different temperature domains characterize the behavior of the background electrons, as indicated in Fig. 4. In the first domain, where $T_{rm} \leq T_e < T_*$, conducting electrons are degenerate. Correspondingly, the heat capacity C_e is a linearly increasing function of the electron temperature and the electrical resistivity η is almost constant, equal to its room-temperature value η_{rm} . In this region $\alpha=0$ and $\beta=1$, and, according to Eq. (23), the temporal evolution of the electron temperature is given by (in this T_e range, $t_k=0$)

$$T_e(t) = T_{rm} \left(1 + 2 \frac{\eta_{rm} j^2}{C_{rm} T_{rm}} t \right)^{1/2}; \quad (32)$$

this solution is valid until the time t_{f1} , at which T_e becomes equal to T_* ,

$$t_{f1} = \frac{1}{2} \frac{C_{rm} T_{rm}}{\eta_{rm} j^2} \left[\left(\frac{T_*}{T_{rm}} \right)^2 - 1 \right]. \quad (33)$$

In the second domain, for $T_* \leq T_e < T_F$, the electrons are still degenerate, i.e., the heat capacity is still a linear function of T_e , but the electrical resistivity is quadratically increasing with the electron temperature, due to electron-electron collisions, then $\alpha=2$ in Eq. (21). Correspondingly, $\alpha-\beta=1$, then, from Eq. (24), the electron temperature is now given by

$$T_e(t) = T_* \exp \left[\frac{\eta_0 j^2}{C_* T_*} (t - t_{f1}) \right], \quad (34)$$

where $C_* = C_{rm}(T_*/T_{rm})$. This solution is valid till the time t_{f2} , for which $T_e = T_F$,

$$t_{f2} = t_{f1} + \frac{C_* T_*}{\eta_{rm} j^2} \ln \left(\frac{T_F}{T_*} \right). \quad (35)$$

The third domain, $T_F \leq T_e < T_{**}$, is characterized by the constant ideal heat capacity C_{id} , Eq. (22), and the constant maximum electrical resistivity ($\alpha=0$). Since $\alpha-\beta=0$, T_e is linearly increasing with time, Eq. (23), that is,

$$T_e(t) = T_F \left[1 + \frac{\eta_{max} j^2}{C_{id} T_F} (t - t_{f2}) \right]. \quad (36)$$

This linear increase of the electron temperature holds until the time t_{f3} , when $T_e = T_{**}$,

$$t_{f3} = t_{f2} + \frac{C_{id} T_F}{\eta_{max} j^2} \left(\frac{T_{**}}{T_F} - 1 \right). \quad (37)$$

Finally, in the last domain, for $T_e \geq T_{**}$, $\alpha-\beta=-3/2$, and, again from Eq. (23), one finds the solution for the heating of an ideal hot electron plasma,

$$T_e(t) = T_{**} \left[1 + \frac{5}{2} \frac{\eta_{max} j^2}{C_{id} T_{**}} (t - t_{f3}) \right]^{2/5}; \quad (38)$$

the final temperature T_{efin} will be reached at the time

$$t_{fin} = t_{f3} + \frac{2}{5} \frac{C_{id} T_{**}}{\eta_{max} j^2} \left[\left(\frac{T_{efin}}{T_{**}} \right)^{5/2} - 1 \right]. \quad (39)$$

To conclude the presentation of the heating model we note that one can also take into account the increase of the background electron density due to thermal (collisional) ionization, with an appropriate choice of the parameter β . However, this will not change qualitatively the results.

C. A numerical example-Al target

In order to make quantitative estimates of the background electron heating in a metal by the return current induced by the current of fast electrons, we apply the model presented in this section to the case of aluminum (Al). This material is widely used in laser-solid experiments [43] and its physical characteristics are well known. It has the background electron density of $1.8 \times 10^{23} \text{ cm}^{-3}$, and consequently T_F is about 11.6 eV. According to the free electron gas model, we can fit the experimental value of the room electrical resistivity ($\eta_{rm} \approx 2.5 \times 10^{-6} \text{ ohm cm}$) by choosing the constant $g_0 = 3$ in Eq. (27). Then, from Eq. (29), electron-electron collisions become the dominant scattering process in Al (in the nonequilibrium regime $T_e \gg T_i$) at the electron temperature $T_* \approx 0.95 \text{ eV}$. The estimate for the maximum value of the electrical resistivity given by Eq. (30) is in fairly good agreement with the experimental measurements of $\sim 2.2 \times 10^{-4} \text{ ohm cm}$ [43]. We also choose $T_{**} = 100 \text{ eV}$ [42,43] as the electron temperature above which the electrical resistivity η is governed by the Spitzer law. Finally, we estimate the fast electron current density as $j \sim n_{0h} e c$; for $n_{0h} = 10^{20} \text{ cm}^{-3}$, we have $j \approx 5 \times 10^{11} \text{ A/cm}^2$. Assuming the hot electron mean energy of 1 MeV, this current corresponds to the fast electron energy flux of $5 \times 10^{17} \text{ W/cm}^2$. It can be obtained with the laser intensity of $2.5 \times 10^{18} \text{ W/cm}^2$, assuming the conversion efficiency of 20%.

By using these parameters, one can estimate the time evolution of the background electron temperature. It takes about a few femtoseconds to reach $T_* \sim 1 \text{ eV}$, about $\sim 15 \text{ fs}$ to reach $T_F \sim 10 \text{ eV}$, and $\sim 40 \text{ fs}$ to achieve $T_{**} \sim 100 \text{ eV}$. So background electrons should be heated up to $\sim 100 \text{ eV}$ in

about 60 fs by the return current originated by the fast electrons flowing in the solid metal target. This time is much less than the time scales typical for processes such as electron-ion relaxation or thermal conduction, as previously discussed.

Moreover, one can use Eq. (39) to estimate the time required by the background electrons to be heated up to a given temperature. For example, the temperature 500 eV would be reached after ~ 1 ps, while after 6 ps the electron temperature would be ~ 1 keV. This estimate qualitatively agrees with the temperatures reported in the numerical simulations [39,40]. This time must be compared with the duration of the fast electron current, which is ultimately related also to the duration of the laser pulse. Moreover, after a few picoseconds, some of the effects neglected might become significant, slowing down the heating process. For a pulse of hundred of femtoseconds, we can estimate the final cold electron temperature to be of the order of 500 eV–1 keV, this last value being an upper limit, above which in any case a more accurate treatment of the heating process would be necessary. On the other hand, if the pulse duration is shorter (a few tens of femtoseconds), the duration of the fast electron current is shorter as well, and the heating of the background population is expected to be less effective. In accordance with the proposed scenario, for Al one can infer a final background electron temperature of the order of ~ 100 eV.

IV. DISCUSSION: TWO-TEMPERATURE EFFECTS ON ION ACCELERATION

We have shown that, depending on the relative value of the cold and hot electron pressures, the resulting self-consistent electric field, generated at the rear side of the foil target, can be significantly influenced from the presence of the cold electron population. If the cold pressure is sufficiently high to be comparable with the hot electron pressure, its most remarkable effect is the production of a peak in the electric field, localized near the vacuum solid interface, and extended inside and outside the target over few cold Debye lengths. These features are important for ion detachment and acceleration [34].

A. Ion detachment and ionization

The first stage of the ion acceleration process in laser-solid interaction must consist in the creation of ions and in their detachment from the solid. These ions originate from the bulk solid and/or from a lower-density proton-rich layer (typically several atomic layers) of contaminants and impurities, always present in these experiments [12,14], if no special measure to clean the surface (by resistive or chemical heating) is undertaken [18,17].

In order to better understand the physical processes involved, let us first consider the “clean” situation, in which no contamination layer is present, and look for the consequences following from our model. We know from our previous analysis that in the two-electron temperature system, the electric field on the rear side can penetrate the target falling down almost exponentially over a few cold Debye lengths λ_{dc} , Eq. (15), which is a very short distance, comparable with the distance between the atomic layers in the

lattice. In the one-temperature case, the electric field is much more symmetric with respect to the target surface and it falls down over some Debye lengths λ_d [see, for example, the approximate explicit solution inside the target, Eq. (5) with $a=0$]. Then, taking into account the presence of a two-temperature electron population, the penetration of the self-consistent electric field inside the solid target is greatly reduced if compared with the one-temperature case ($n_c=0$). It can potentially detach (depending on its strength) only a few bulk layers.

The maximum electric field is of the order of several MV/ μm . It largely exceeds the effective electric field required to detach an ion from the atomic layer, which is of the order of the ion binding energy in the solid (a few eV) divided by the ion charge and the interatomic distance, that is, roughly ~ 0.02 MV/ μm . It also exceeds the threshold for field ionization. Another source of ionization are the collisions of heated background electrons.

We conclude that the self-consistent electric field at the rear surface is sufficient to detach and ionize the ions in few target atomic layers. Typically, a single layer contains about 10^{16} ions/ cm^2 . Taking into account the angular spread of the hot electron beam, θ , we can estimate the transverse extension of the hot electron cloud on the rear surface as $R_e \approx d/2 + l \tan \theta$, where d is the laser focal spot diameter and l is the target thickness. Assuming $l=100 \mu\text{m}$ and $\theta=25^\circ$, we find $R_e \approx 50 \mu\text{m}$. This estimate of R_e agrees with the results of recent optical measurements of the rear side of the target [45]. The number of ions detached from a single layer would be of the order of 7×10^{11} , and then the total number of ions detached by the electric field from a few layers would be about several times 10^{12} .

Since $\lambda_{dc} \propto \sqrt{T_c}$, we should expect that a stronger heating of the cold electron population should result in a larger number of bulk layers detached. As discussed in Sec. III B and below, the cold electron temperature increases with the pulse duration. For example, assuming a cold electron density of about 10^{23} cm^{-3} , $\lambda_{dc} \approx 0.2$ nm with the cold electron temperature T_c of 100 eV, while $\lambda_{dc} \approx 0.7$ nm if $T_c=1$ keV. Therefore the number of accelerated ions should increase with the laser pulse duration.

Consider now the early dynamics of the electric field after the detachment of the first target layers. One can reasonably assume that during the time of the order of the pulse duration, the energy of the hot electron population (directly delivered by the laser pulse) is approximately constant. The structure of the self-consistent electric field does not considerably change, as long as the number of ions accelerated remains smaller than the total number of hot electrons. However, the peak of the electric field (which is initially localized at the solid-vacuum interface) “moves backwards,” inside the target as more and more layers are detached. It moves with a velocity of the order of the ion-acoustic velocity c_s , in which the electron temperature is of the order of the mean electron temperature $\langle T_{0e} \rangle$ as defined in Eq. (10). Then, the distance Δx the electric field penetrates into the target is the maximum between $c_s t_p$ (t_p being the laser pulse duration time) and the cold electron Debye length λ_{dc} . Consequently, it defines the number of layers detached. Since in solid tar-

gets $a \equiv n_{0c}/n_{0h} \gg 1$, $\langle T_{0e} \rangle$ is about T_h/a when the hot electron pressure is greater than the cold electron pressure, while its value is about $bT_h = T_c$ in the opposite situation. Whatever the case, we can assume that $\langle T_{0e} \rangle$ is at most $\sim \text{keV}$. Consequently, for most materials, the ion-acoustic velocity is typically $\sim 10^7$ cm/s. With short pulses (tens of femtoseconds), Δx is then about few nanometers, while for longer pulses (hundreds femtoseconds), Δx can be even tens nanometers. As far as the detachment is concerned, the motion of the electric field inside the target during the pulse duration can change the order of magnitude of the layer thickness detached when “long” pulses are used. This is in qualitative agreement with the recent observations by Spencer *et al.* [46].

We can now qualitatively describe the effects of the contamination layer. Since usually the density of the contamination layer is lower than solid density, the effective charge of contaminant ions is also low and then, at least as a first approximation, one can assume that they do not alter the structure of the electric field described in Sec. II. Thus, the contaminant layer is simply “superimposed” on the clean system, and the maximum electric field is then localized at the solid-contaminant interface. As already noted, the contaminant layer contains always protons: being the lighter ions, protons are the first to be accelerated. If their number is enough to significantly screen the electrostatic field, they inhibit the acceleration of the heavy bulk ions, present in the target (and also the heavy ions from the contamination layer itself). Let us assume a value for the contaminant layer density of the order of 10^{22} cm $^{-3}$. For the same parameters used before ($l = 100$ μm and $\theta = 25^\circ$, $R_e \approx 50$ μm) the number of protons per unit length of the contamination layer is about 10^{17} - 10^{18} cm $^{-1}$. With a layer thickness of about 10 nm, the total number of protons in the contamination layer should be about 10^{11} - 10^{12} . With the aim of estimating their effects, one must compare these numbers with the total number of hot electrons, which is typically of the order of several times 10^{13} , depending on the parameters of the system. From these simple evaluations we conclude that, in order to completely “screen” the target, the contamination layer should be at least of the order of several tens of nanometers, that is, thicker than the value usually assumed in the experiments (even if it is not exactly known). This is why one expects that for usual experimental conditions, the detachment and acceleration of the bulk ions from the target are important complementary processes.

The target itself can contain protons (typically if plastic targets, constituted of H and C, are used). In this case we expect the total number of protons accelerated to be several times, in order of magnitude, the number obtained in similar conditions but with metallic targets, assuming there are no protons inside the target in this last case. This behavior was observed in experiments [13], namely, with similar laser pulse parameters and target thickness, using a CH target it was measured a number of protons of about 3.5×10^{13} , while with an Au target, the protons measured were five times less, even if the maximum proton energies obtained were similar in both cases.

B. Ion acceleration

Note, first of all, that the maximum electric field value in the one-temperature case, where the effect of the heated bulk electrons are not considered, is $E(0) = \sqrt{2/e}(T_h/e\lambda_{dh})$ while, from our analysis, the maximum electric field produced by a two-temperature distribution is never less than $\sqrt{2}T_h/e\lambda_{dh}$ (provided that $a \gg 1$). The difference is almost a factor 2. What is more important, this value might be enhanced if the cold electron pressure is greater than the pressure of the laser generated fast electrons. Hence, the finding of the conditions where the cold electron heating is most effective, is of practical interest. Both target design and laser parameters seem to be important in this context. In metals, the cold electron density can be considered approximately as a given quantity. It may grow due to thermal ionization, but more slowly than the cold electron temperature. Then, the pressure increases mainly due to the heating process, as long as the fast electron current is present in the target. A lower limit for its duration is the pulse duration. Therefore, in experiments with long pulses (hundreds of femtoseconds), the order of magnitude of the heating time should be \sim picoseconds. An estimate for the background temperature in these conditions, for aluminum, is ~ 1 keV and consequently the ratio between the cold and hot electron temperatures is of the order of $b = T_c/T_h \sim 10^{-3}$. The density of conduction electrons, at this temperature is of the order of 10^{24} cm $^{-3}$, due to thermal ionization. Then, the ratio a of the densities turns out to be of the order of or greater than $\sim 10^4$, if we assume a value for the mean hot electron density of about 10^{20} cm $^{-3}$.

Thus, for long enough pulses the background electron pressure is of the same order as or even greater than the hot electron pressure. Correspondingly, the presence of the very localized and enhanced peak of the electric field should affect the detachment and ionization process, and also the acceleration of ions. First, the increased electric field results in a more effective layer detachment; second, more layers can be detached; third, the presence of the peak distribution affects the temporal evolution of the acceleration, providing an “injector” capable of accelerating the ions over a very short distance (nm) up to energies of the order of few keV.

On the contrary, for shorter pulses (few tens of femtoseconds) the heating of the background population should be less effective. Assuming again that the fast electron current and the pulse duration are of the same order, in aluminum we expect a final temperature of the order of ~ 100 eV. In these conditions the background electron pressure does not exceed the hot electron pressure.

In order to quantitatively estimate the maximum ion energy, the knowledge of the temporal evolution of the electric field profile is required [28,35]. Moreover, as already pointed out in Sec. II A, even in the stationary isothermal model of ion expansion, some physical “truncation mechanism” has to be introduced in order to avoid the divergent behavior of the electrostatic potential at infinity. Nevertheless, some general conclusions about ion acceleration can be derived.

Let us consider the typical situation of multispecies ion composition of the target, where ions with various charge states are present, in particular, protons and heavier ions

from the contaminant layer and/or the bulk material. The acceleration time t_{acc} is the same for all ion species. It can be limited by two mechanisms. First, if the total number of protons is large enough, they can alter the charge density distribution with their motion. This happens in the time taken by a proton to move across a hot Debye length (about $1 \mu\text{m}$). For a MeV proton this time is of the order of 0.2–0.5 ps. The heavier ions are less important because protons are more rapidly accelerated due to their lighter mass. Second, the ion acceleration can be terminated also because of the energy depletion of the hot electron population, the source of the electric field on the rear surface. After the laser pulse terminates, the hot electrons lose their energy by adiabatic cooling expansion or by collisions. According to the numerical simulations [47], this happens in a picosecond time scale. The faster time scale associated with these processes determines the upper limit for the ion acceleration time t_{acc} at the rear surface, which should be no more than a few picoseconds, according to our estimates.

During the time t_{acc} , every ion species acquires a momentum $p_i \approx Ze \int_0^{t_{acc}} E(t) dt$, and consequently the final energy $\mathcal{E}_i = p_i^2/2m_i$, where m_i is the ion mass. From these considerations we conclude that final ion energies are related and, in particular, the ratio between ion and proton maximum energies should scale as Z^2/A_i , where $A_i \equiv m_i/m_p$ is the ion mass number. This scaling seems to agree with the observations [14,16].

Finally, the formation of a localized peak in the electric field profile also reveals itself as an important issue in the double-layer mechanism of laser-induced ion acceleration [35,48]. In this approach, a foil of heavy ions is coated on the rear side with a thin layer of light ions (typically, protons) which provides the charge separation. During the acceleration of the light ions, heavy ions may be assumed at rest and the desired proton energy spectrum is controlled by means of the variation of the layer thickness. The presence of a localized electric field peak influences the choice of the ion layer thickness since we have seen that it would extend over few cold electron Debye lengths (several nanometers), inside and outside the target. The different electric field profile influences also the final ion energy spectrum. Then, in this case, in order to produce a narrow proton energy distribution, the coating thickness should be less than a few cold Debye lengths.

V. CONCLUSIONS

In this paper we have developed an analytical theory which presents the description of the self-consistent electrostatic field (the *sheath* field) in a target with a multitempera-

ture electron population. The heating of the background electron population due to the presence of a return current in the system is included in the model.

The electric field is significantly influenced by the cold electron population: first, this population determines the penetration of the electric field inside the target, which occurs over a distance of a few cold electron Debye lengths; second, if the cold electron pressure is greater than the hot electron pressure, the maximum value of the electric field increases.

The cold electron pressure increases due to the Ohmic heating induced by the return current in the target. Since the heating process is related to the presence of the return current, it is more effective for longer pulses. According to our estimations for a standard Al target, using very short laser pulses (tens of femtoseconds) the final cold electron temperature is of the order of 100 eV, while a temperature of the order of keV is achievable for a hundred femtoseconds pulses.

We have shown that these properties can significantly influence the ion detachment, the ionization, and finally the ion acceleration. These processes are shown to be controlled by means of the heating rate of the background electrons. In order to increase this heating rate, a search for target materials with extraordinary resistivity and presenting an anomalously fast heating seems to be an interesting issue, with the aim of providing an efficient ion acceleration, especially with short laser pulses. Together with the relevant target design, this may have a fundamental significance and potential applications in the implementation of ion accelerators driven by table-top lasers.

In order to build a more satisfactory theory on ion acceleration when an ultraintense and ultrashort laser pulse interacts with a thin solid target, it is important to investigate quantitatively the effects of other phenomena, such as the role played by possible front-surface acceleration mechanisms, and, in the framework of the rear acceleration processes, deviation from the stationary description (time dependence of the hot electron temperature and time evolution of the accelerating field), the effects related to a multidimensional geometry (divergence of the ion beam, role of the self-generated magnetic field), the electron recirculation in the thin foil, and the consequences of a nonstepwise initial ion distribution.

ACKNOWLEDGMENTS

M.P. wishes to acknowledge the hospitality of the Centre Lasers Intense et Applications (CELIA), where most of the work was carried out, and of the University of Bordeaux 1 for supporting his visit to France. Part of this work was carried out in the framework of INTAS Project No. 01-0233.

-
- [1] M. Borghesi *et al.*, Phys. Plasmas **9**, 2214 (2002).
 [2] M. Roth *et al.*, Phys. Rev. Lett. **86**, 436 (2001).
 [3] V.Yu. Bychenkov *et al.*, Plasma Phys. Rep. **27**, 1017 (2001).
 [4] M. Temporal, J.T. Honrubia, and S. Atzeni, Phys. Plasmas **9**, 3098 (2002).

- [5] F.P. Boody, R. Hoepfl, and H. Hora, Laser Part. Beams **14**, 443 (1996).
 [6] H. Haseroth and C.E. Hill, Rev. Sci. Instrum. **67**, 1328 (1996).
 [7] K. Krushelnik *et al.*, IEEE Trans. Plasma Sci. **28**, 1184 (2000).
 [8] M.I.K. Santala *et al.*, Appl. Phys. Lett. **78**, 19 (2001).

- [9] K. Nemoto *et al.*, Appl. Phys. Lett. **78**, 595 (2001).
- [10] S.V. Bulanov and V.S. Khoroshkov, Plasma Phys. Rep. **28**, 453 (2002).
- [11] E. Fourkal *et al.*, Med. Phys. **29**, 2788 (2002).
- [12] E.L. Clark *et al.*, Phys. Rev. Lett. **84**, 670 (2000).
- [13] R.A. Snavely *et al.*, Phys. Rev. Lett. **85**, 2945 (2000).
- [14] M. Allen *et al.*, Phys. Plasmas **10**, 3283 (2003).
- [15] A. Maksimchuk *et al.*, Phys. Rev. Lett. **84**, 4108 (2000).
- [16] E.L. Clark *et al.*, Phys. Rev. Lett. **85**, 1654 (2000).
- [17] M. Zepf *et al.*, Phys. Rev. Lett. **90**, 064801 (2003).
- [18] M. Hegelich *et al.*, Phys. Rev. Lett. **89**, 085002 (2002).
- [19] A.J. Mackinnon *et al.*, Phys. Rev. Lett. **86**, 1769 (2001).
- [20] A.V. Gurevich, L.V. Pariiskaya, and L.P. Pitaevskii, Zh. Eksp. Teor. Fiz. **49**, 647 (1965) [Sov. Phys. JETP **22**, 449 (1966)].
- [21] C. Sack, and H. Schamel, Phys. Rep. **156**, 311 (1987).
- [22] M. Widner, I. Alexeef, and W.D. Jones, Phys. Fluids **14**, 795 (1971).
- [23] J.E. Crow, P.L. Auer, and J.E. Allen, J. Plasma Phys. **14**, 65 (1975).
- [24] J.S. Pearlman and R.L. Morse, Phys. Rev. Lett. **40**, 1652 (1978).
- [25] J. Denavit, Phys. Fluids **22**, 1384 (1979).
- [26] A.V. Gurevich and A.P. Meshcherkin, Zh. Eksp. Teor. Fiz. **80**, 1810 (1981) [Sov. Phys. JETP **53**, 937 (1981)].
- [27] Y. Kishimoto, K. Mima, T. Watanabe, and K. Nishikawa, Phys. Fluids **26**, 2308 (1983).
- [28] P. Mora, Phys. Rev. Lett. **90**, 185002 (2003).
- [29] L.M. Wickens, J.E. Allen, and P.T. Rumsby, Phys. Rev. Lett. **41**, 243 (1978).
- [30] L.M. Wickens, and J.E. Allen, J. Plasma Phys. **22**, 167 (1979).
- [31] A.V. Gurevich, D. Anderson, and H. Wilhelmsson, Phys. Rev. Lett. **42**, 769 (1979).
- [32] M.A. True, J.R. Albritton, and E.A. Williams, Phys. Fluids **24**, 1885 (1981).
- [33] V.F. Kovalev, V.Yu. Bychenkov, and V.T. Tikhonchuk, Pis'ma Zh. Eksp. Teor. Fiz. **74**, 12 (2001) [JETP Lett. **74**, 10 (2001)]; Zh. Eksp. Teor. Fiz. **122**, 263 (2002) [JETP **95**, 226 (2002)].
- [34] V.T. Tikhonchuk, Phys. Plasmas **9**, 1416 (2002).
- [35] V. Yu. Bychenkov, V. N. Novikov, D. Batani, and V. T. Tikhonchuk (unpublished).
- [36] M. Passoni and M. Lontano, Laser Part. Beams (to be published).
- [37] J. R. Davies, Phys. Rev. E **68**, 056404 (2003).
- [38] A.P. Kanavin, I.V. Smetanin, V.A. Isakov, Y.V. Afanasiev, B.N. Chichkov, B. Wellegehausen, S. Nolte, C. Momma, and A. Tunnerman, Phys. Rev. B **57**, 14698 (1998).
- [39] J. J. Honrubia (unpublished).
- [40] L. Gremillet, G. Bonnaud, and F. Amiranoff, Phys. Plasmas **9**, 941 (2002).
- [41] N. W. Ashcroft and N. D. Mermin, *Solid State Physics* (Holt, Rinehart and Winston, New York, 1976); A. A. Abrikosov, *Fundamentals of the Theory of Metals* (North-Holland, Amsterdam, 1988).
- [42] K. Eidmann, J. Meyer-ter-Vehn, T. Schlegel, and S. Huller, Phys. Rev. E **62**, 1202 (2000).
- [43] H.M. Milchberg R.R. Freeman, S.C. Davey, and R.M. More, Phys. Rev. Lett. **61**, 2364 (1988).
- [44] L. Spitzer, Jr., *Physics of Fully Ionized Gases* (Interscience, New York, 1956).
- [45] J.J. Santos *et al.*, Phys. Rev. Lett. **89**, 025001 (2002).
- [46] I. Spencer *et al.*, Phys. Rev. E **67**, 046402 (2003).
- [47] D.W. Forslund and J.U. Brackbill, Phys. Rev. Lett. **48**, 1614 (1982); T. Zh. Esirkepov *et al.*, Pis'ma Zh. Eksp. Teor. Fiz. **70**, 80 (1999) [JETP Lett. **70**, 82 (1999)]; H. Ruhl *et al.*, Fiz. Plazmy **27**, 387 (2001) [Plasma Phys. Rep. **27**, 363 (2001)].
- [48] T.Zh. Esirkepov *et al.*, Phys. Rev. Lett. **89**, 175003 (2002).